A complete hydro-climate model chain to investigate the in uence of sea surface temperature on recent hydroclimatic variability in subtropical South America (Laguna Mar Chiquita, Argentina)

Magali Troin, Mathieu Vrac, Myriam Khodri, Caya Daniel, Christine Vallet-Coulomb, Eduardo L. Piovano, Florence Sylvestre

A complete hydro-climate model chain to investigate the influence of sea surface temperature on recent hydroclimatic variability in subtropical South America (Laguna Mar Chiquita, Argentina)

Magali Troin[1,2] · Mathieu Vrac[3] · Myriam Khodri[4] · Daniel Caya[2] · Christine Vallet-Coulomb[1] · Eduardo Piovano[5] · Florence Sylvestre[1]

Abstract During the 1970s, Laguna Mar Chiquita (Argentina) experienced a dramatic hydroclimatic anomaly, with a substantial rise in its level. Precipitations are the dominant driving factor in lake level fluctuations. The present study investigates the potential role of remote forcing through global sea surface temperature (SST) fields in modulating recent hydroclimatic variability in Southeastern South America and especially over the Laguna Mar Chiquita region. Daily precipitation and temperature are extracted from a multi-member LMDz atmospheric general circulation model (AGCM) ensemble of simulations forced by HadISST1 observed time-varying global SST and sea-ice boundary conditions from 1950 to 2005. The various members of the ensemble are only different in their atmospheric initial conditions. Statistical downscaling (SD) is used to adjust precipitation and temperature from LMDz ensemble mean at the station scale over the basin. A *coupled* basin-lake hydrological model (*cp*HM) is then using the LMDz-downscaled (LMDz-SD) climate variables as input to simulate the lake behavior. The results indicate that the long-term lake level trend is fairly well depicted by the LMDz-SD-*cp*HM simulations. The 1970s level rise and high-level conditions are generally well captured in timing and in magnitude when SST-forced AGCM-SD variables are used to drive the *cp*HM. As the LMDz simulations are forced solely with the observed sea surface conditions, the global SST seems to have an influence on the lake level variations of Laguna Mar Chiquita. As well, this study shows that the AGCM-SD-*cp*HM model chain is a useful approach for evaluating long-term lake level fluctuations in response to the projected climate changes.

Keywords LMDz · Statistical downscaling · Hydrological modeling · Lake level variability · Southeastern South America

1 Introduction

Amongst the world's sub-continental regions, Southeastern South America (SESA which includes Uruguay, southern Brazil, Paraguay and northern Argentina) has shown one of the largest hydroclimatic trends of the 20th century (Liebmann et al. 2004; Barros et al. 2008; IPCC 2013). While the first three quarters of the 20th century were affected by prolonged droughts, the western portion of SESA experienced an unprecedented humid phase between the early 1970s and the mid-1980s (Garcia and Vargas 1998; Garcia and Mechoso 2005). This wet period has shown increased precipitation and higher frequency and severity of extreme hydrologic events in SESA (Genta et al. 1998; Berbery and Barros 2002; Camilloni and Barros 2003; Planchon and Rosier 2005). These recent hydroclimatic changes in SESA have impacted the socio-economic activities of the region;

✉ Magali Troin
troin@cerege.fr; troin.magali@ouranos.ca

1 CNRS, IRD, CEREGE UM34, Aix-Marseille Université, 13545 Aix-en-Provence, France

2 Department of Construction Engineering, École de technologie supérieure, Université du Québec, 1100 Notre-Dame Street West, Montreal, QC H3C 1K3, Canada

3 Laboratoire des Sciences du Climat et de l'Environnement (LSCE-IPSL) CNRS-CEA-UVSQ, Centre d'étude de Saclay, Orme des Merisiers, Bat. 701, 91191 Gif-Sur-Yvette, France

4 LOCEAN/IPSL, IRD/CNRS/MNHN/UPMC, Sorbonne Université, Tour 45-55, 4 place Jussieu, 75252 Paris Cedex 5, France

5 CICTERRA-CIGeS, Universidad Nacional de Córdoba, Av. Velez Sarsfield 1611, X5016GCA, Córdoba, Argentina

mainly those related to agriculture and hydroelectric power generation (Barros et al. 2000; Pasquini et al. 2006). In addition to the observed trend towards increased precipitation throughout the last century, precipitation over SESA has exhibited considerable year-to-year variability (Vera and Silvestri 2009). Several studies have documented the influence of the ocean–atmosphere coupling expressed by El Niño and the Southern Oscillation (ENSO) signal on the interannual variability of precipitation over South America (Grimm et al. 2000; Vera et al. 2006a; Taschetto and Wainer 2008; Krishnamurthy and Misra 2010). Findings from these works indicate that in general ENSO's warm phases are related to positive precipitation anomalies over SESA. However, precipitation in SESA contains another mode(s) of variability at the decadal to multi-decadal scales (expressed in low-frequency variability; Robertson and Mechoso 2000; Berbery and Barros 2002). A number of hypotheses of ocean heat balance through anomaly patterns in sea surface temperature (SST) fields have been proposed to explain this low-frequency variability in precipitation; these include decadal changes in the ENSO-Southern Annual Mode (SAM) correlation (Vera and Silvestri 2009), the influence of the Pacific Decadal Oscillation (PDO) mode (Barreiro 2010) associated with the role of the mid-1970s North Pacific climate shift (Huang et al. 2005), and the impact of tropical Atlantic sea surface temperature (SSTA) as the tropical component of the Atlantic Multi-decadal Oscillation (AMO; Seager et al. 2010). Nevertheless, these hypotheses remain open-ended, as the nature of low-frequency precipitation variability has not yet been completely explained.

In order to assess regional vulnerability, a better understanding of 20th century hydroclimatic trends throughout SESA is required to cope with the projected effects of climate change. In particular, the physical mechanisms leading to these trends in the 1970s and governing the interannual and lower frequency of hydroclimatic variability in the region must be better understood. For the past few decades, efforts to investigate the links between climate variability and oceanic forcing have been based on both observations and atmospheric global climate model (AGCM) data. For instance, AGCMs with forced SSTs were used to assess the models' ability to depict variability in precipitation over South America (Seager et al. 2010), and to analyse the role of SST changes in the year-to-year variability of precipitation or in precipitation increase over SESA (Junquas et al. 2012, 2013). Recently, Barreiro et al. (2014) performed simulations with an AGCM forced by different SST conditions to describe the role(s) of the global oceans and the land–atmosphere interaction on summertime interdecadal variability in the region. While much attention is being given to the influence of oceanic driving on precipitation variability, few studies have focused on the signature of SST anomalies on the hydrological changes observed in SESA. Over the SESA catchments, studies based on time series of river streamflow data have produced conflicting results; mainly due to the use of different time periods and geographical locations. Robertson et al. (2001) provided indications that decadal streamflow fluctuations in the Paraná Basin may be partially predictable by the ENSO-range fluctuations. Pasquini et al. (2006) identified apparent near-decadal and near-bidecadal climatic signatures in streamflow records in central Argentina. However, they concluded that it was difficult to draw a connection between those signatures and the ENSO signal. More recently, Vera and Díaz (2014) used CMIP5 simulations to provide significant evidence that precipitation changes observed in SESA over the last century are at least partially explained by the human-induced greenhouse gases increment. Conclusions from these studies point the need for further investigations to discern whether 20th century hydroclimatic changes in SESA are influenced by forcing from SST anomalies and/or from anthropogenic forcing (i.e., human-induced climate change). The present study intends to contribute to the potential role of oceanic forcing on 20th century hydroclimatic variability observed in the region, combining a SST-forced AGCM with a *coupled* basin-lake hydrological model (*cp*HM).

Laguna Mar Chiquita Basin in central Argentina is sensitive to high- and low-frequency changes in regional hydrology (Pasquini et al. 2006) and, therefore, to climate variability in SESA. The lake basin was shown to be sensitive to recent hydroclimatic changes observed in the region. This terminal saline lake of a 127,000 km^2 closed watershed saw its level increasing sharply in the 1970s. This persistent high-level period is unprecedented over the last millennium according to paleolimnological studies (Piovano et al. 2009). In recent years, considerable attention has been focused on the driving factors of the 1970s lake level rise in hopes of deciphering the roles of local climatic and anthropogenic (e.g., land cover/land use) influences on hydrological changes. Troin et al. (2010) conducted the first comprehensive study of Laguna Mar Chiquita's response to regional climate and runoff variability, using a lake model. They reported the dominant role of increased discharge in the Rio Sali-Dulce Basin on the lake level rise that occurred in the 1970s. Then, Troin et al. (2012) investigated the impact of climate and land cover changes on the Sali-Dulce Basin's streamflow using the physically-based Soil Water Assessment Tool (SWAT) model. They pointed out that precipitation increase was the major driver of the hydrological change that occurred over the Sali-Dulce Basin during the 1970s. The results they reported for the Sali-Dulce Basin are relevant to Laguna Mar Chiquita, as this sub-catchment's streamflow is the main forcing factor of lake level variations (Troin et al. 2010). The combined use of the lake model and SWAT made it possible to develop a *coupled* basin-lake hydrological model (*cp*HM) that could adequately simulate

the main modes of lake level variations throughout the 20th century (including the sharp rise in level observed during the 1970s) without having to consider land cover/land use changes (Troin et al. 2012). These previous studies were limited to the influence of local climate forcing on lake level variations since the *cp*HM was driven solely by observed data derived from local stations. Assumptions about the likely connections between oceanic forcing and recent high- and low-frequency changes observed in the lake region is thought to be better addressed using SST-forced AGCM outputs to drive the *cp*HM.

The present study focuses on investigating the role of oceanic forcing in driving multi-decadal variability in the hydroclimate of the Laguna Mar Chiquita region, by using the *cp*HM driven by large-scale climate variables derived from SST-forced AGCM to simulate lake behavior in the recent past. A specific objective is to assess whether Laguna Mar Chiquita can be thought of as a recorder of global climate forcing from the SST in the region. This assessment, if verified, has potentially far-reaching implications for a better understanding of the links between recent climate variability and hydrological changes in SESA. More specifically, the response of the AGCM when forced by observed time-varying global SST is investigated. The selected AGCM is the LMDz, the atmospheric component of the IPSL-CM4 version of the Institut Pierre Simon Laplace-Coupled Model (Marti et al. 2005). IPSL-CM4 is one of the World Climate Research Program (WCRP)-CMIP3 models used to perform climate change simulations in the 4th IPCC assessment report (IPCC 2007). The added benefits of applying a statistical correction to LMDz precipitation and temperature data are evaluated using a statistical downscaling model, named CDF-t for 'Cumulative Distribution Function—transform' (Michelangeli et al. 2009). The raw and statistically downscaled precipitation and temperature derived from the LMDz are then given to SWAT to simulate streamflow in the Sali-Dulce Basin. Finally, the resulting SWAT simulations are introduced into the lake model in order to evaluate the *cp*HM's ability, driven by SST-forced AGCM outputs, to reproduce the variability in Laguna Mar Chiquita levels throughout the 20th century.

The paper is organized as follows: Sect. 2 describes the study area and the selected LMDz regions. The methodology's three-step process is presented in Sect. 3. Section 4 depicts the key results of the model chain, and a discussion and the conclusions follow in Sect. 5.

2 Material

2.1 Study area

Laguna Mar Chiquita (30°54′S–62°51′W) is a hydrologically closed terminal lake with a catchment area extending from 26°S to 32°S and from 62°W to 66°W (Fig. 1). Three rivers feed the lake (Fig. 1). The main surface water input comes from the Rio Sali-Dulce, which contributed 92 % of the lake-level rise in the 1970s (Troin et al. 2010). The Sali-Dulce Basin is located in the northwestern part of the lake basin and spans an area of 23,810 km^2 from 26°S to 28°S and 64°W to 66°W (Fig. 1). Other minor inflows to the lake stem from the southwestern part of the lake basin. The lake system has no surface outlet and evaporation is the only water loss, favored by the lake's pan-like shape (Troin et al. 2010).

The lake basin presents a warm-temperate to subtropical climate from south to north. Annual precipitation and temperature varies from 806 mm and 18 °C around the lake to 1300 mm and 20 °C towards the Sali-Dulce Basin. Orographic precipitation exceeding 1500 mm per year occurs in the northern part of the Sali-Dulce Basin. Most precipitation falls in the wet season from December to March. The dry season lasts from June to August.

The major feature of South America's seasonal climate variability is the development of the South American Monsoon System (SAMS), which extends south from the tropical continental region during the austral summer. It connects the tropical Atlantic Inter Tropical Convergence Zone (ITCZ) with the South Atlantic Convergence Zone (SACZ) through large-scale atmospheric circulation displaying a low-level jet (Zhou and Lau 1998). The South American low-level jet drives the moisture transport in SESA throughout the year (Vera et al. 2006b). By contrast, the SAMS's weak convective activity in austral winter is accompanied by reduced precipitation in South America except in the eastern part of SESA, where the circulation of the southeast trade wind brings moisture associated with local precipitation (Barros et al. 2002).

2.2 Data

Two types of daily climate data/output sets are compiled for the purpose of hydrologic modeling experiments: observed-station data and climate model outputs.

2.2.1 Observational data

Daily precipitation and maximum and minimum temperatures data in the Sali-Dulce Basin come from the National Climatic Data Center (NCDC) and the CLARIS LPB project database (http://www.claris-eu.org/). The data is compiled from five stations covering the 1973–2005 period over the catchment. Station P2 has the longer series, from 1950 to 2005 (Fig. 1).

2.2.2 AGCM outputs

The AGCM-simulated daily precipitation and temperature are generated with the LMDz, the atmospheric global

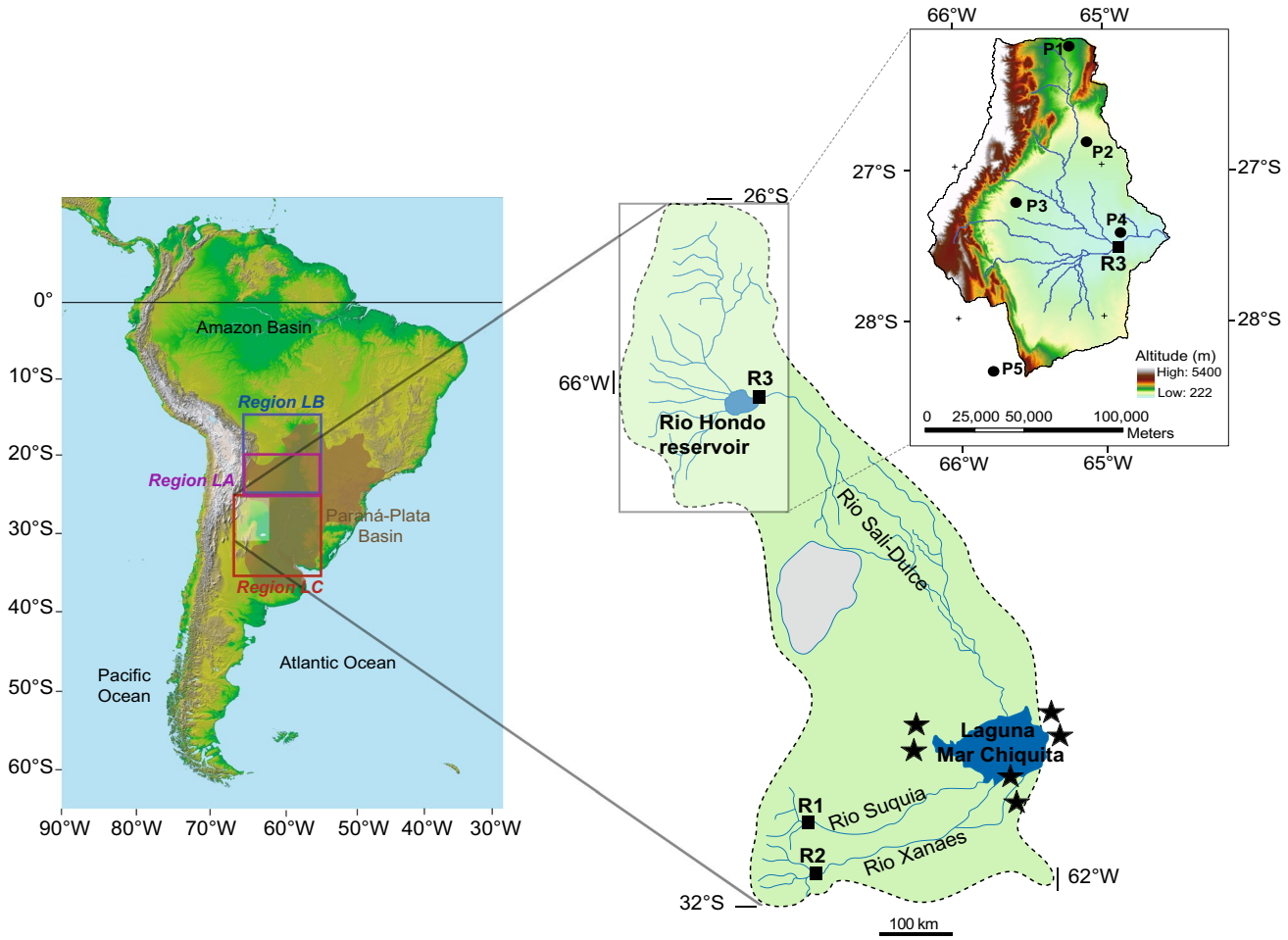

Fig. 1 Location of Laguna Mar Chiquita Basin west of the Parana-Plata Basin and the three LMDz regions (Regions *LA*, *LB* and *LC*). The *enlarged view* shows the Sali-Dulce Basin in the northern part of the lake basin. Observed data used for SWAT come from meteorological stations P1 to P5 and one gauging station R3 at the Rio Hondo reservoir outlet. Data used for the lake water balance model (Troin et al. 2010) come from six meteorological stations around the lake (*black stars*) and three gauging stations (R1–R3)

circulation model developed at Laboratoire de Météorologie Dynamique (Marti et al. 2005). LMDz has a uniform resolution of 3.75° in longitude and 2.5° in latitude, with 19 vertical atmospheric layers (Hourdin et al. 2006). We used an LMDz 10-member ensemble forced by monthly HadISST1 global observed sea surface temperature (SST) and sea ice cover (SIC) as ocean surface boundary conditions over the 1950–2005 period. Each simulation member differs only by the initial state of the atmosphere, as determined by ten different states for January 1st. Since the LMDz ensemble simulations are forced by observed time-varying SST, averaging the ensemble of AGCM simulations is used to detect the signal from the white noise associated with atmosphere internal variability (or inter-member variability) and to keep the SST-forced AGCM response. The LMDz 10-member ensemble mean is therefore considered in further analyses to focus on the SST forced signal.

2.2.3 Selection of AGCM regions

The gap between the spatial resolution and scale of AGCMs is a critical challenge for proper simulations of hydrological processes at the catchment scale (Chen et al. 2013; Troin et al. 2015). In addition, because of the coarse resolution of the AGCM, the patterns of climate circulation, such as those derived from the grid points in the AGCMs over the regional area of interest, can significantly differ from those actually observed from the meteorological stations. This constitutes another difficulty in the use of climate model outputs to feed a *cp*HM. A common approach to resolve the scale discrepancy between the AGCMs and the resolution required for hydrological studies is to downscale the AGCM output. One of the prerequisites for some of the downscaling procedure is to determine regions in the sub-domain of the AGCMs that provide the best estimate of the observed climate patterns. The determination of the

regions in the AGCMs' sub-domain takes into account both geographical and climatological factors: the regions must be in a geographical location close to the catchment area and offer the most realistic representation of observed climate variables.

The selection of LMDz regions is thus carried out over the sub-domain extending from 13°S to 35°S in latitude and from 52°W to 68°W in longitude that incorporates the Sali-Dulce Basin (26°S–28°S and 64°W–66°W; Fig. 1). This sub-domain will be referred to as the SD-Domain. The Root Mean Square Error (*RMSE*) is used to measure the average difference between observed values of precipitation or temperature and simulated values for the same variables taken from LMDz over the 55-year period (1950–2005). The *RMSE* is computed as

$$RMSE(x,y,m) = \sqrt{\frac{1}{N}\sum_{m=1}^{N}\left(S_{x,y,m} - O_m\right)^2} \quad (1)$$

where O_m is the averaged mean monthly seasonal cycle computed using all the meteorological stations over the 55-years period; $S_{x,y,m}$ is the mean climatological monthly value for each LMDz grid points (x,y) over the SD-Domain over the 55 simulated years; and N corresponds to 12 months. The objective here is to evaluate the AGCM skills in reproducing the mean climatology at each grid point as compared to observed temperature and precipitation over the SD-Domain. It is commonly accepted that the lower the *RMSE*, the lower the distance between the AGCM outputs and the observations, the better the model performance. Based on this criterion, the LMDz regions that better agree with the mean seasonal cycle over the Sali-Dulce Basin are selected for the downscaling procedure.

Figure 2 compares the *RMSE* spatial structure between observational data and the LMDz for precipitation (grey shading), maximum (orange contours) and minimum temperatures (blue contours) over the SD-Domain. The LMDz region extending between 20°S–25°S and 55°W–65°W (hereafter labelled region LA; Fig. 2) shows low *RMSE* for the three climate variables. To get a broader image of the LMDz's simulated climate performance over the Sali-Dulce Basin and to evaluate the lake response to the climate features north and south to the actual Sali-Dulce Basin, two other regions are selected. These two regions are referred to as regions LB (from 15° to 25°S and 55° to 65°W) and LC (from 25° to 35°S and 55° to 67°W). Regions LA and LB are located north of the Sali-Dulce Basin, while region LC encompasses the actual geographical area of the lake basin including the Sali-Dulce Basin identified by the grey box (Fig. 2). The selected LMDz regions are used to explore the influence of oceanic forcing in modulating the hydroclimatic variability in the lake region as simulated by the SST-forced AGCM. They also serve as sensitivity experiments to discern the processes that drive the climate patterns over the Sali-Dulce Basin and ultimately the lake level fluctuations.

The mean annual cycles for precipitation, and minimum and maximum temperatures in the selected LMDz regions are displayed in Fig. 2b–d. The amplitudes of the mean annual cycles of precipitation and temperature agree with observations for region LA, although small differences do exist. Compared to region LA, region LB overestimates precipitation in austral summer and autumn, and shows a warm bias in austral winter. Even though region LC overlaps the observations made in the basin, the amplitude of the mean annual cycle of precipitation is underestimated and that of temperature is overestimated. Consequently, both lower latitude regions in LMDz show better skill than region LC at replicating the observed mean annual climate cycle in the Sali-Dulce Basin.

3 Methods

3.1 Projecting AGCM outputs to catchment level

AGCMs are able to simulate important aspects of the current climate, among them many patterns of climate variability observed across a range of time scales. However, for most hydrological-relevant variables, AGCMs do not currently provide reliable information on scales below about 200 km (e.g. Maraun et al. 2010). This large scale is too coarse for a realistic representation of most hydrological processes that act over a large range of scales, including very fine and local ones. Therefore, spatial downscaling and statistical post-processing of AGCM outputs are necessary for a meaningful translation of climate simulations to the relevant hydrological scale. Downscaling AGCM outputs can be done with either a statistical or a dynamical approach. The statistical downscaling models determine statistical relationships between large-scale climate information or data and local/regional variables, whereas dynamical downscaling employs regional climate models based on physical equations of the regional dynamic of the atmosphere. These two fundamental downscaling approaches have strengths and limitations that have been widely discussed in the literature (e.g. Fowler et al. 2007; Maraun et al. 2010). In the present study, we focus on the use of statistical model for downscaling AGCM simulations.

Our procedure is as follows: the large-scale climate variables (e.g., precipitation and temperature) extracted from the selected LMDz regions are translated to local-scale station observations in the catchment using the SD method. For this study, the SD method relates large-scale precipitation and temperature to local-scale precipitation and temperature

Fig. 2 Comparison of LMDz with observed climatology (1950–2005): **a** Relative Root Mean Square Error (RMSE) for precipitation totals (*grey shading*) in millimeters, minimum (*blue contour*) and maximum (*orange contour*) temperatures in degrees. The *grey boxes* show the stations' location in the Sali-Dulce Basin. LMDz regions LA, LB, LC are shown *boxed*; averaged mean seasonal cycle for (**b**) precipitation totals in millimeters, **c** minimum and **d** maximum temperatures in degrees over LMDz regions LA, LB, LC. The averaged mean seasonal cycles based on the observational data in the Sali-Dulce Basin are also specified

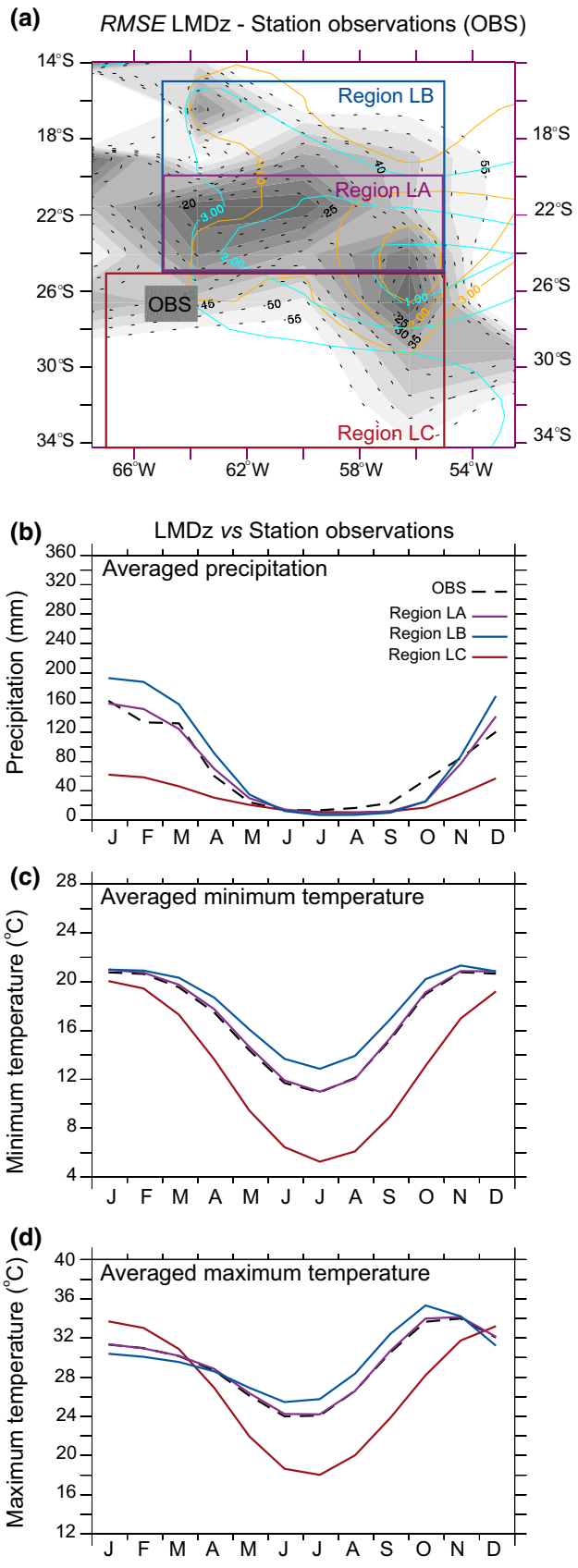

through the 'Cumulative Distribution Function—transform' (CDF-t) method (Michelangeli et al. 2009). The SD method relies on the notion of the Cumulative Distribution Function F (CDF) of a random variable X which corresponds to the probability that a random realization of X is equal to or lower than a given value x: $F(x) = Proba\ (X \leq x)$. The CDF-t method can be perceived as a variant of the quantile–quantile method (Déqué 2007). It is based on the assumption that there exists a transformation T allowing the translation of the CDF of an AGCM variable (e.g., temperature or precipitation) into the CDF representing a local-scale variable (e.g., temperature or precipitation for a given station observation). CDF-t accounts for the change in the large-scale CDF from the historical to the future period required in a changing climate context. Technical details and general philosophy of the CDF-t method are provided in Michelangeli et al. (2009) and Vrac et al. (2012).

For precipitation, the method involves two steps:

1. A wet-day threshold is determined from daily large-scale precipitation time series such that the frequency of large-scale precipitation occurrences matches the observed frequency. In the observations, a wet day is defined as a day that receives 1 mm or more of rain. A threshold (t_S) is calculated to obtain as many large-scale wet days (i.e., with large-scale precipitation intensities higher than t_S) as the number of observed wet days at station S. In other words, if F_S is the CDF of precipitation at station S, and if F_L is the CDF of the large-scale precipitation, t_S is then determined such that $F_L(t_S) = F_S(1)$;
2. The large-scale precipitation values of the days with precipitation occurrences (i.e., with precipitation $\geq t_S$ mm) are downscaled using CDF-t.

Daily distributions of large-scale minimum and maximum temperatures derived from the LMDz are directly downscaled using CDF-t, as the variable is continuous and without a lower bound in this study. The procedure is applied for all seasons together, for both precipitation and temperature.

For both variables, CDF-t is calibrated over the 1973–1989 period where the most complete observed dataset is available. The CDF-t method is then applied to downscale data over two validation periods extending from 1950 to 1972 and from 1990 to 2005. Note that before 1972, CDF-t is evaluated based on data from one station only (see Sect. 2.2.1).

3.2 Catchment-scale hydrological modeling

The downscaled data from LMDz are given to the Soil Water Assessment Tool (SWAT) model for streamflow simulation in the Sali-Dulce Basin. SWAT is a physically-based semi-distributed model that operates on a daily time step (Arnold et al. 1998). It represents the spatial variability of land use, soil types and management practices by dividing the watershed into multiple hydrologic response units (HRUs), each representing a unique combination of land cover, soil and slope. The climate variables required to run SWAT are daily precipitation and daily maximum and minimum air temperatures.

The watershed hydrology in SWAT is simulated in two steps. The first step is the land phase of the hydrologic cycle, which calculates each HRU's water balance to determine the amount of water available for each sub-basin's main channel at a given time step. The second step is the channel routing, which determines the progress of water through the river network towards the basin outlet (Neitsch et al. 2002). The HRU water balance is expressed as,

$$W_t = W_o + \sum_{i=1}^{t} (P_i - Q_{isurf} - ET_i - w_{iseep} - Q_{igw}) \quad (2)$$

where W_t is the soil moisture content at time t; W_o is the initial soil moisture content; P_i is the precipitation on day i; Q_{isurf} is the surface runoff on day i; ET_i is the evapotranspiration on day i; w_{iseep} is the percolated water through the soil profile on day i; and Q_{igw} is the groundwater flow on day i. All terms are expressed in mm of water.

The Laboratorio de Hidráulica at the Universidad Nacional de Córdoba provided monthly discharges for the 1950–2005 period at the Hondo Station located below the Rio Hondo reservoir (Fig. 1). The different components of SWAT applied to the Sali-Dulce Basin are described in Troin et al. (2012). A more detailed description of the model components is presented in Neitsch et al. (2005). A comprehensive review of SWAT applications is given in Gassman et al. (2007).

3.3 Lake-scale hydrological modeling

To simulate Laguna Mar Chiquita's monthly level variations, SWAT-simulated Rio Sali-Dulce discharges (Q_{R3}) driven by raw and downscaled data from LMDz regions are integrated into the lake water balance model developed by Troin et al. (2010). The dynamic lake water balance equation at the monthly time scale Δt is given by

$$\frac{\Delta V}{\Delta t} = A(V)(P - E) + Q_{in} - \gamma \quad (3)$$

with

$$Q_{in} = Q_{R1} + Q_{R2} + Q_{R3} \quad (4)$$

where ΔV is the lake volume variation (m^3); A is the lake area (m^2) as a function of lake volume V; P is on-lake precipitation (m/month) estimated from six rainfall stations located around the lake (Fig. 1); E is evaporation from the lake surface (m/month) calculated using the Complementary Relationship Lake Evaporation (CRLE) model (Morton 1983; DosReis and Dias 1998); Q_{in} is the water inflow from the catchment (m^3/month); Q_{R1} and Q_{R2} are the discharges of the two southern rivers; Q_{R3} is the Rio Sali-Dulce discharge corresponding to 90 % of Q_{in}; and the γ parameter refers to water loss by evapotranspiration in the un-gauged surfaces around the lake (m^3/month) as discussed in Troin et al. (2010). The corresponding lake level is estimated as a function of lake volume, $h = f(V)$, following the morphometric relationship established using lake bathymetry (Hillman 2003). More details of the implementation of this model for Laguna Mar Chiquita are provided in Troin et al. (2010).

4 Results

4.1 Statistical downscaling performance for different climates

The SD method's performance is first assessed with respect to its applicability under non-stationary climatic conditions, as the studied period exhibits contrasting precipitation regimes (Troin et al. 2012). The calibrated SD method over the wet 1973–1989 period ($P_{1973–1989}$ = 1106 mm/year) is evaluated over two drier periods of 22 years ($P_{1950–1972}$ = 740 mm/year) and 15 years ($P_{1990–2005}$ = 853 mm/year).

Overall, the daily mean and standard deviation values of precipitation and temperature generated by the SD method are closer to the observed than the raw data values over both validation periods (Table 1), which indicates an informative downscaling of global climate to the catchment level by CDF-t under contrasting climatic conditions. In particular, with statistical downscaling (hereafter SD), regions LA and LB are in better agreement with observations than region LC-SD for the total amount, the daily mean and standard deviation of precipitation over the validation periods. The

Table 1 Comparison of statistically downscaled and observed precipitation, maximum and minimum temperatures for the three LMDz regions (LA, LB and LC) over the validation periods (bracket values refer to raw data)

Data source	Precipitation (mm)			Maximum temperature (°C)		Minimum temperature (°C)	
	Mean	σ	Total	Mean	σ	Mean	σ
1990–2005							
Region LA-SD	2.3 (2.3)	0.7 (0.7)	847 (819)	27.1 (32.3)	0.9 (0.8)	14.6 (19.8)	0.8 (0.7)
Region LB-SD	2.3 (2.6)	0.8 (0.9)	849 (977)	27.1 (29.9)	0.9 (0.8)	14.6 (18)	0.8 (0.8)
Region LC-SD	2.4 (1.1)	0.6 (0.7)	877 (367)	27 (27.5)	0.8 (0.7)	14.5 (13.6)	0.6 (0.6)
OBS	2.3	0.7	853	27.6	0.8	14	0.8
1950–1972							
Region LA-SD	1.6 (2.2)	0.8 (0.7)	592 (802)	26.6 (31.4)	0.9 (0.8)	14.0 (20.1)	0.8 (0.8)
Region LB-SD	1.8 (2.5)	0.9 (0.8)	665 (955)	26.6 (29.1)	0.9 (0.8)	14.0 (17.2)	0.8 (0.7)
Region LC-SD	1.3 (1.0)	0.6 (0.7)	465 (361)	26.6 (33)	0.8 (0.8)	14.0 (13.2)	0.6 (0.7)
OBS	2	0.8	740	27.1	0.8	13.7	0.8

Note that SD is the acronym used for the statistical downscaling method

Table 2 Seasonal explained variance (%) of daily statistically downscaled precipitation (calculated on the log-values of the positive data), maximum and minimum temperatures for the three LMDz regions (LA, LB and LC) over the validation periods (bracket values refer to the percentage of explained variance for raw data)

	Data source	Season	Precipitation	Temperature	
				Maximum	Minimum
1990–2005	Region LA-SD	DJF	34 (33)	9 (7)	8 (5)
		JJA	39 (37)	11 (9)	13 (11)
	Region LB-SD	DJF	25 (23)	8 (6)	13 (9)
		JJA	39 (37)	8 (7)	9 (6)
	Region LC-SD	DJF	17 (14)	8 (6)	13 (10)
		JJA	35 (32)	10 (8)	11 (7)
1950–1972	Region LA-SD	DJF	33 (30)	10 (8)	9 (7)
		JJA	41 (38)	15 (11)	26 (21)
	Region LB-SD	DJF	27 (22)	9 (6)	15 (12)
		JJA	35 (27)	10 (7)	11 (9)
	Region LC-SD	DJF	17 (13)	9 (8)	15 (13)
		JJA	38 (33)	12 (10)	13(12)

Note that SD is the acronym used for the statistical downscaling method

DJF December to February, *JJA* June to August

SD method's performance under different climates results from the fact that the associated raw data in both LMDz regions are less biased and more coherent with observations than they are in region LC (Fig. 2). All LMDz regions perform similarly well at reproducing the daily mean and standard deviation temperature values over both validation periods after statistical downscaling (Table 1).

The SD method's performance is then assessed with respect to its ability to reproduce the daily variability of precipitation and temperature in austral summer (DJF) and winter (JJA) seasons. This is done by estimating the seasonal explained variance (E) for each validation period as:

$$E = \left[\frac{\sum_{i=1}^{N} (S_i - \bar{O})^2}{\sum_{i=1}^{N} (O_i - \bar{O})^2} \right] \times 100 \quad (5)$$

where N corresponds to the number of days in austral summer or winter in the validation period; O_i refers to the observed data value for day i in austral summer or winter in the validation period; $\bar{O}$ is the mean daily observed value in austral summer or winter over the validation period; and S_i is the downscaled value for day i in austral summer or winter over the validation period. E is the ratio (in percentage) of the simulation's variance over the observed data variance. E is not biased if the data follow a normal, or Gaussian distribution, such as for temperature. Since daily precipitation is usually considered 'log-normally' distributed (i.e., the logarithm of strictly positive daily precipitation values is normally distributed; see Maraun et al. 2010; Carreau and Vrac 2011), E is applied on the log-values of the positive precipitation data only. Marked differences between LMDz regions are evident over the validation

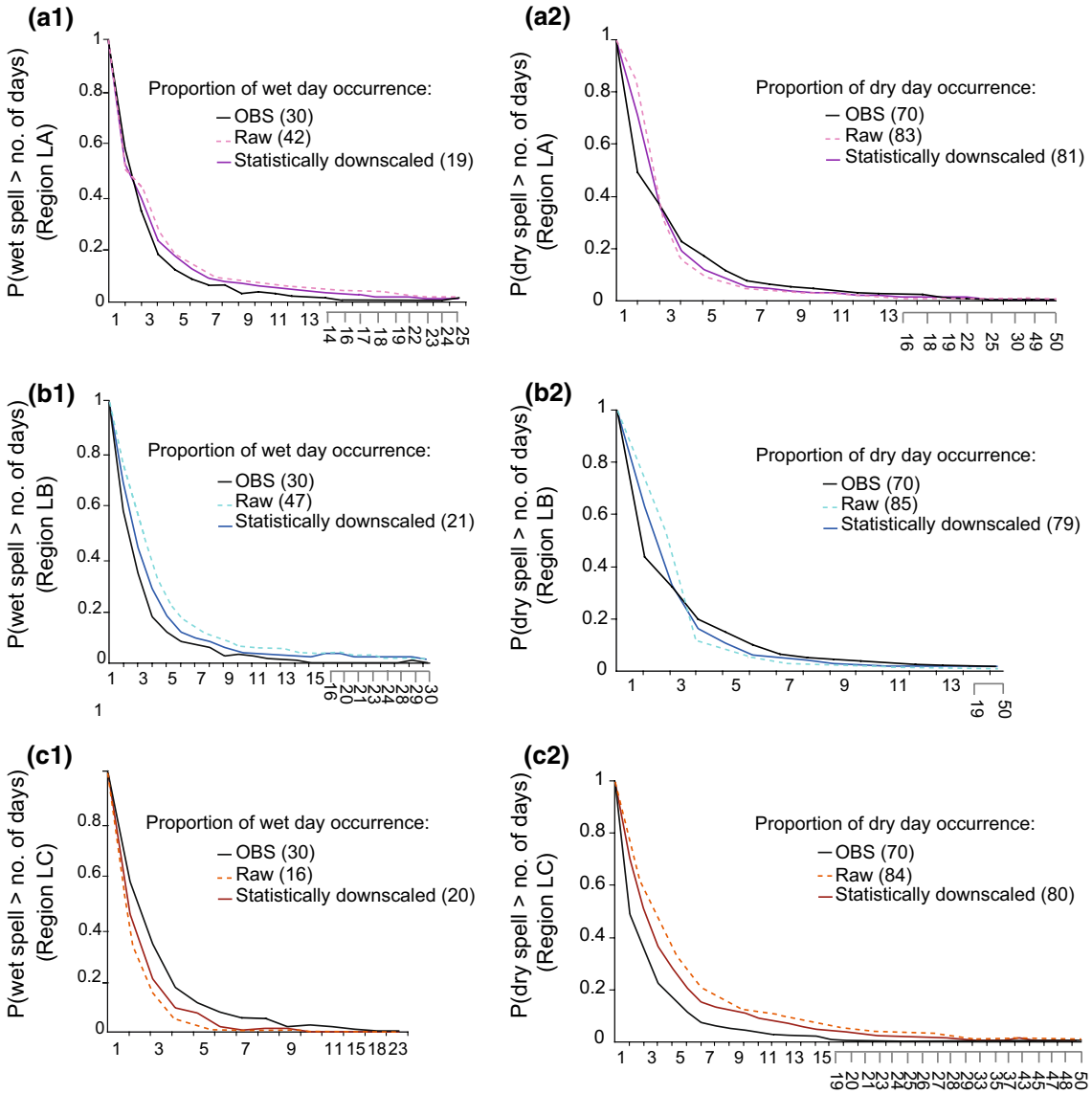

Fig. 3 Comparison of wet (*first column*) and dry (*second column*) spell probabilities in observed precipitation to that of raw and statistically downscaled precipitation from **a** LMDz region LA, **b** LMDz region LB and **c** LMDz region LC over the 1990–2005 validation period. The proportion of wet and dry day occurrences is also specified

periods (Table 2). In both seasons, region LA-SD produces the largest *E*-values for precipitation and for maximum temperature. This is less obvious for minimum temperature, where regions LB-SD and LC-SD provide the highest *E*-value in austral summer. As a general result, statistically downscaled precipitation and temperature in LMDz regions are more accurate in austral winter because of the much larger value of *E*. However, the SD method's accuracy remains similarly consistent in both seasons due to the similar changes of *E* with respect to raw data, underlining the absence of seasonal bias in the SD method.

The probabilities of the duration of wet and dry spells for LMDz simulated and observed precipitation over the two validation periods are shown in Figs. 3 and 4. Dry spells are defined as a number of consecutive days without rainfall, and consecutive days with rainfall are called wet spells. In this study we used a threshold of 1 mm day^{-1} to distinguish between a wet and a dry day. We can see that LMDz-SD precipitation consistently reproduced the probability of observed wet and dry spells, even for small values of probabilities corresponding to long periods. A tendency to underestimate (overestimate) the wet (dry) spell probability is observed for the LMDz-SD regions over the validation periods. The proportion of dry day occurrences is better represented than that of wet day occurrences.

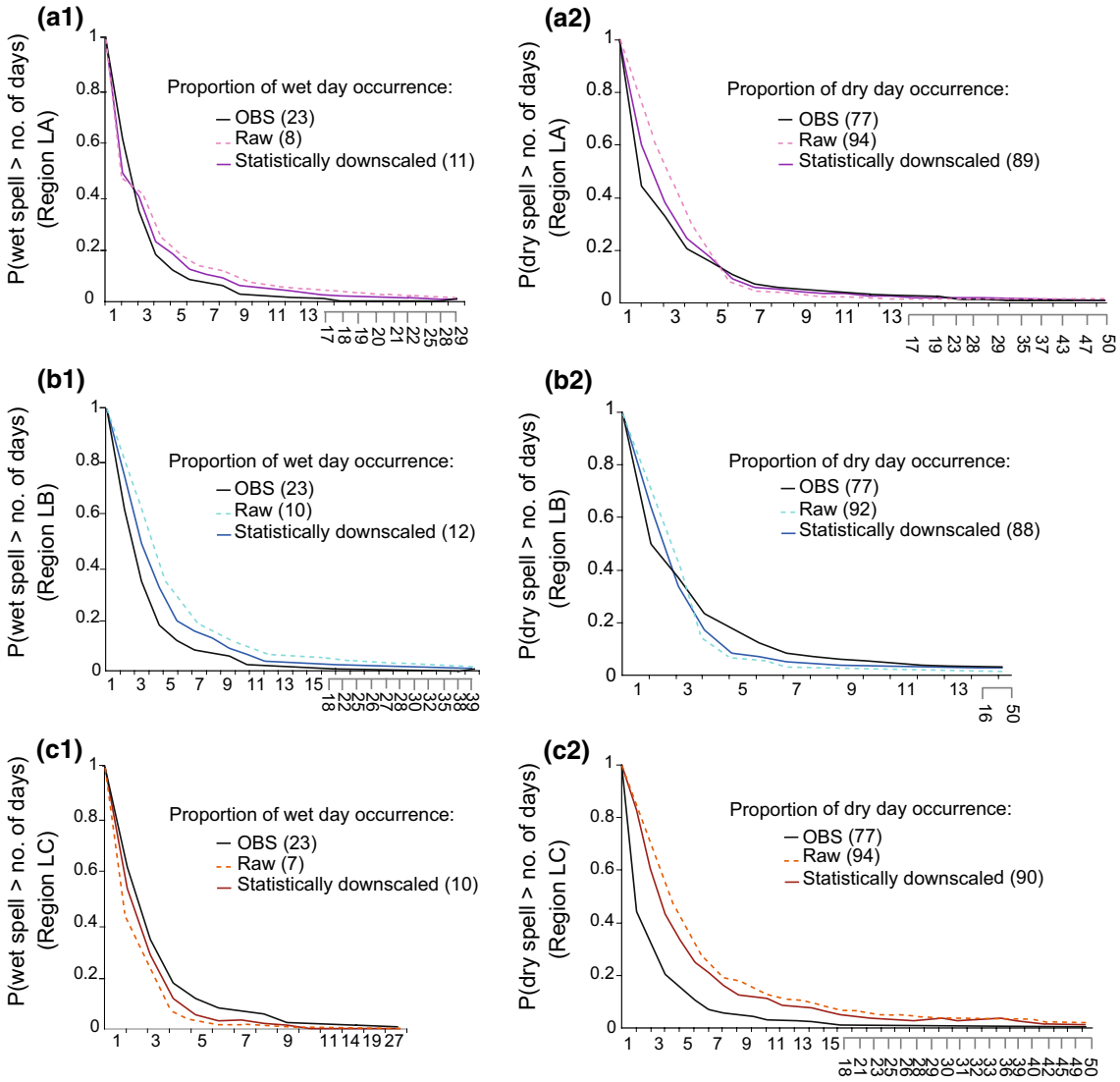

Fig. 4 Comparison of wet (*first column*) and dry (*second column*) spell probabilities in observed precipitation to that of raw and statistically downscaled precipitation from **a** LMDz region LA, **b** LMDz region LB and **c** LMDz region LC over the 1950–1972 validation period. The proportion of wet and dry day occurrences is also specified

4.2 Simulation of long-term streamflow variations

Further to the SD evaluation, the performance of the AGCM-SD-*cp*HM model chain is evaluated by its ability to reproduce the Sali-Dulce Basin's hydrology. Because we are interested in long-term trends and because the catchment's streamflow is governed by precipitation variability (Troin et al. 2012), the predictability of interannual and decadal variability in streamflow is analyzed. In this respect, the present analysis aims to provide indications of the consistency of simulations of the streamflow variability when the SST-forced AGCM data are used as inputs to SWAT. The analysis is conducted by comparing the LMDz-SD simulated discharges with observed time series in terms of long-term mean annual flows filtered with a 3-year moving average.

Figure 5 shows that the 3-year moving average filter on regions LA-SD and LB-SD simulates annual discharge indexes and displays multi-year oscillations, making four dominant hydrological cycles appear: two cycles with approximately a 16-year (hereafter 16Y) period (i.e., Cycle I: 1957–1972; Cycle II: 1973–1988 in Fig. 5) and two cycles with about an 8-year (hereafter 8Y) period (i.e., Cycle III: 1989–1996; Cycle IV: 1997–2004 in Fig. 5), both noticeably consistent with observations. Only Cycles I and IV are discernible and well-defined in the region LC-SD-simulated discharges. The interannual streamflow variations superimposed on the 16Y and 8Y cycles in regions LA-SD- and LB-SD-simulated discharges follow the observations when compared to the simulations performed with region LC-SD. In particular, the timing of

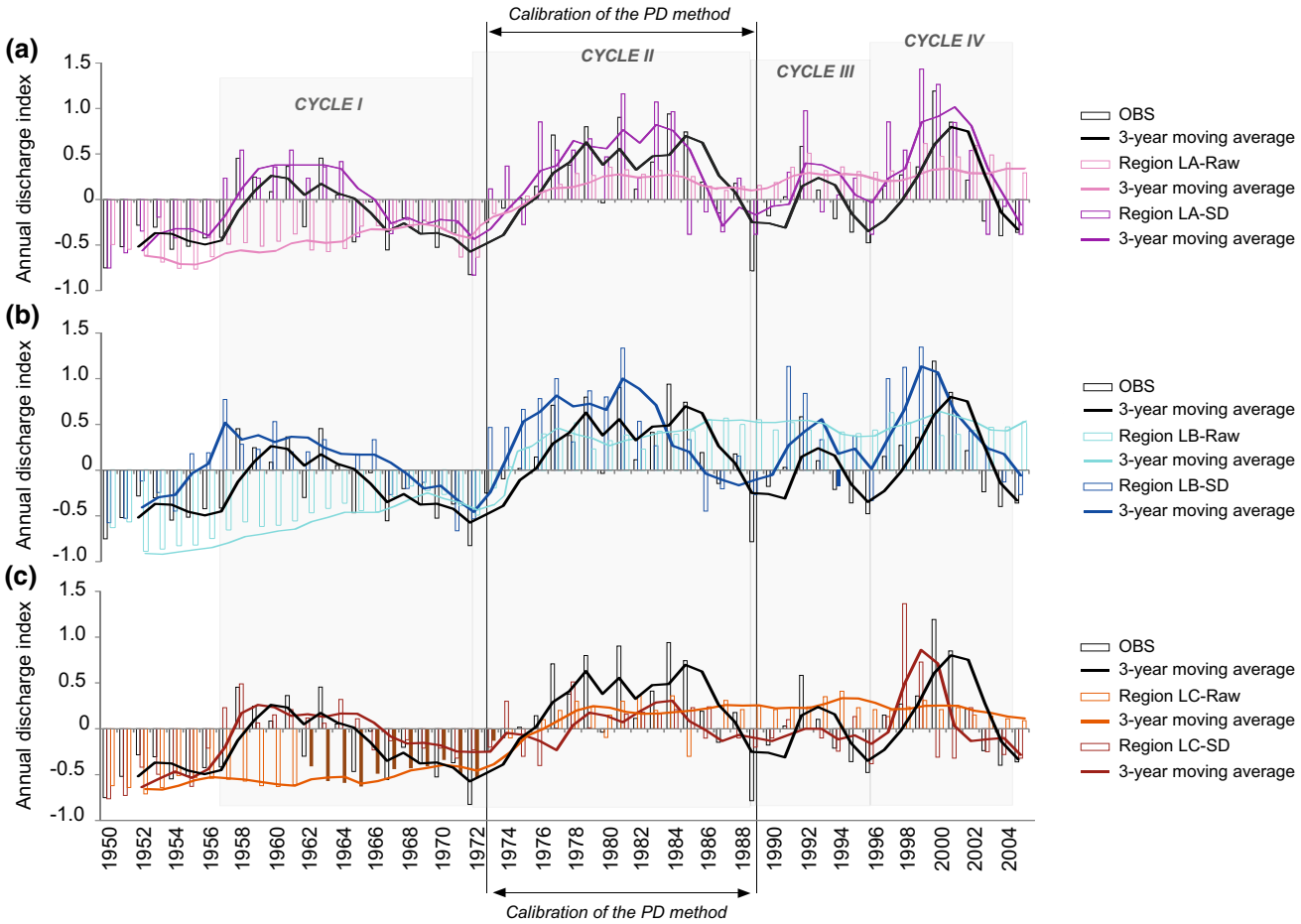

Fig. 5 Annual normalized indexes (I_i) and 3-year moving average for observed and SWAT-simulated discharges using raw and statistically downscaled data from **a** LMDz region LA, **b** LMDz region LB and **c** LMDz region LC over the 1950–2005 period. I_i is estimated using normal standardization formula as $I_i = (X_i - \bar{X})/X$ with X_i and $\bar{X}$ the total and mean annual values respectively. The key hydrological cycles are also specified

the predominantly high annual flows corresponding to the absolute maxima in the 16Y and 8Y cycles after the 1970s are fairly well captured in the regions LA-SD and LB-SD discharge simulations (i.e., 1981, 1992 and 2000 in Fig. 5); but their magnitudes are overestimated.

The analysis of the Nash–Sutcliffe efficiency (*NSE*) criterion confirms our previous results (Table 3): the highest performance in simulating monthly streamflow is observed for regions LA-SD and LB-SD over the calibration ($NSE_{region\ LA\text{-}SD} = 0.56$; $NSE_{region\ LB\text{-}SD} = 0.59$), the 22-year ($NSE_{region\ LA\text{-}SD,22} = 0.50$; $NSE_{region\ LB\text{-}SD,22} = 0.48$) and the 15-year ($NSE_{region\ LA\text{-}SD,15} = 0.49$; $NSE_{region\ LB\text{-}SD,15} = 0.50$) validation periods, with a better prediction of peak flow and baseflow, and a more realistic total volume simulation (Q_s/Q_o). The average magnitude of SWAT-simulated discharges between the wet calibration and dry validation periods in regions LA-SD and LB-SD is maintained below 10 %, supporting the relevance of the SD method for downscaling AGCM outputs under contrasting climatic conditions.

4.3 Simulation of long-term lake level fluctuations

The hydrological experiments are completed by combining the Rio Sali-Dulce discharges as simulated by SST-forced AGCM-SD into the lake model in order to simulate the long-term variability of level fluctuations in Laguna Mar Chiquita. To avoid any bias resulting from the hydrological modeling process, the simulated lake levels obtained from the SWAT-simulated discharges driven by observed meteorological data are considered as the references for further analysis (bold black curve; Figs. 6 and 7). The curves of observed lake level variations (gray curve in Fig. 6) and of simulated lake levels using observed Rio Sali-Dulce discharges (brown curve in Fig. 6) illustrate the propagation of uncertainties. Three sources of uncertainties are considered in this study: (1) *climatic uncertainties* related to the AGCM itself (i.e., internal variability of the climate system when forced with observed sea surface conditions and model imperfections); (2) *statistical uncertainties* based on

Table 3 SWAT performance using statistically downscaled data derived from the three LMDz regions (LA, LB and LC) over the calibration and validation periods of the PD method (bracket values refer to model performance for raw data)

	NSE	*NSE* peak flow[a]	*NSE* base flow[b]	Q_s/Q_o
PD calibration period (1973–1989)				
Region LA-SD	0.56 (0.19)	0.43 (0.17)	0.47 (0.17)	1.13 (0.35)
Region LB-SD	0.59 (0.15)	0.46 (0.14)	0.48 (0.16)	1.15 (0.39)
Region LC-SD	0.39 (0.10)	0.16 (0.05)	0.23 (0.08)	0.79 (0.27)
PD validation period (1990–2005)				
Region LA-SD	0.49 (0.18)	0.38 (0.11)	0.30 (0.19)	1.17 (0.34)
Region LB-SD	0.50 (0.24)	0.41 (0.12)	0.38 (0.25)	1.32 (0.37)
Region LC-SD	0.18 (0.06)	0.09 (0.03)	0.12 (0.04)	1.17 (0.24)
PD validation period (1950–1972)				
Region LA-SD	0.50 (0.21)	0.35 (0.11)	0.34 (0.12)	1.20 (0.54)
Region LB-SD	0.48 (0.21)	0.36 (0.13)	0.37 (0.13)	1.26 (0.52)
Region LC-SD	0.29 (0.16)	0.19 (0.08)	0.28 (0.11)	1.15 (0.24)

Note that SD is the acronym used for the statistical downscaling method

Nash-Sutcliffe efficiency $(NSE) = 1 - \left[\sum_{i=1}^{N} \left(Q_{o_i} - Q_{s_i}\right)^2 / \sum_{i=1}^{N} \left(Q_{o_i} - \bar{Q}_o\right)^2\right]$ with $\bar{Q}_o = \frac{1}{N} \sum_{i=1}^{N} Q_{o_i}$, where Q_o is observed discharge and Q_s is simulated discharge. *NSE* ranges between $-\infty$ and 1, with $NSE = 1$ being the optimal value

[a] Estimated during the high-flow period from January to March

[b] Estimated during the low-flow period from August to October

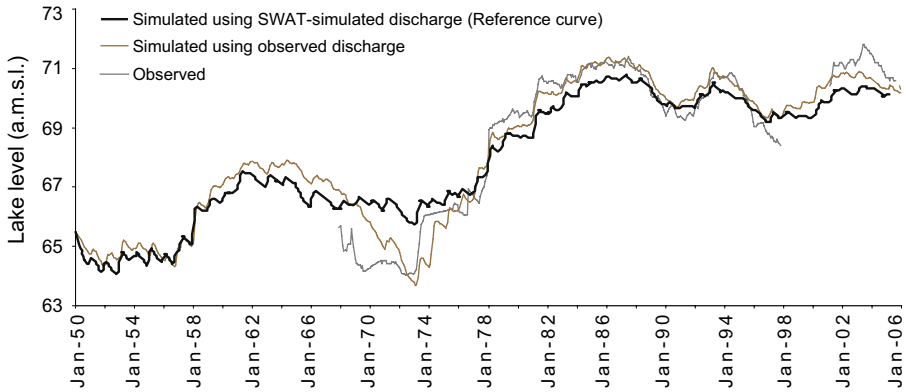

Fig. 6 Observed (*gray line*) and simulated lake levels of Laguna Mar Chiquita over the 1950–2005 period using observed discharges (*brown line*) and SWAT-simulated Rio Sali-Dulce discharges (*bold line*; *reference curve*). Observed lake levels are continuous since 1967 except for a gap between 1997 and 2001 where only three monthly measurements of water level are available

the treatment of the AGCM outputs with the SD method; and (3) *hydrological uncertainties* linked to parameter uncertainty both in SWAT and in the lake water balance model (Fig. 6).

The lake model captures the long-term lake level tendencies fairly well when driven by regions' LA-SD ($r^2 = 0.81$) and LB-SD ($r^2 = 0.79$) simulated discharges (Fig. 7). The dominant 16Y and 8Y cycles, as identified in the reference lake level curve for their time periods, are fully present in regions LA-SD- and LB-SD-simulated lake levels (i.e., Cycle I: 1957–1972; Cycle II: 1973–1988; Cycle III: 1989–1996; Cycle IV: 1997–2004 in Fig. 7). The region LC-SD-simulated lake levels result in a somewhat damped curve and only Cycle I is depicted in the timing of observed high level reproduction in 1961. Superimposed upon the low-frequency variations in lake levels, the moderately high level in the 1960s and the decadal occurrence of high values centered in the 1980s, 1990s and 2000s coincide with maximum values in the 16Y and 8Y cycles (see the reference curve in Fig. 7). The lake level simulations that best reproduce most of the high-level interannual events, both in magnitude and timing, are those performed using regions' LA-SD- and LB-SD-simulated discharges. Nevertheless, the high levels of the 2000s are still shifted earlier in both LMDz-SD-simulated lake level curves; such a time-offset in the 2000s lake level variations is associated quite clearly with annual discharge anomalies in the streamflow simulations over the 1999–2000 period (Fig. 5).

One apparent weakness in all LMDz-SD simulations is the overestimation of the low lake level observed in the late 1960s through the early 1970s. Such difficulties in capturing the low lake level of the 1970s might be a result of the inadequate representation of watershed area rainfall for that period. As discussed in Troin et al. (2012), the

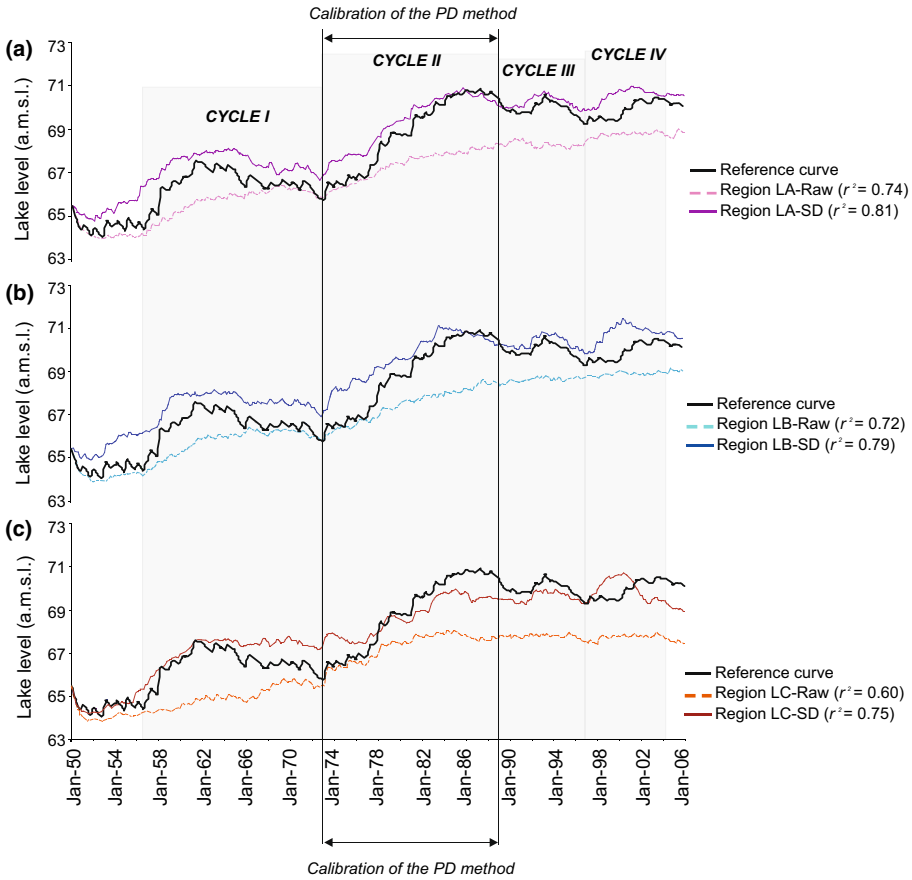

Fig. 7 Simulated lake levels of Laguna Mar Chiquita over the 1950–2005 period using SWATsimulated Rio Sali-Dulce discharges driven by observational data (*reference curve*), raw and statistically downscaled data from **a** LMDz region LA, **b** LMDz region LB and **c** LMDz region LC. The key hydrological cycles are also specified

sole meteorological station available over the 1950–1972 period shows records of extreme precipitation events ($\Delta P/\bar{P}_{1966-1971} = +16\,\%$), and an exceptionally wet year in 1968 ($\Delta P/\bar{P} = +72\,\%$). It is likely that extreme events create a bias in watershed area rainfall estimation over the 1968–1972 period, with an overextension of a local event to the overall region. The uncertainties associated with the inadequate representation of watershed area rainfall that impact on the *cp*HM's results when driven by observed meteorological data are propagated throughout the entire model chain, thereby influencing lake level simulations. Nevertheless, the leading modes of level variations in Laguna Mar Chiquita, such as the 16Y and 8Y cycles, as well as the moderately high lake level of the 1960s, the 1970s level rise, and the high levels in the 1960s, 1980s, 1990s and 2000s are reasonably well captured by the *cp*HM when driven climatically by SST-forced AGCM-SD outputs.

5 Discussion and conclusions

The SESA region has experienced significant variations in its hydrological state over the last century. In central Argentina, the persistence of the 1970s high levels associated with large fluctuations in Laguna Mar Chiquita water levels are indications of this hydroclimatic anomaly observed in the region. It is well known that climate variability on different timescales resulting from ocean–atmosphere interaction modulates precipitation patterns at a regional scale (Nobre et al. 2006). This present study aims to evaluate the role of oceanic forcing in modulating the multi-decadal variability of the hydroclimate in the Laguna Mar Chiquita region, by combining an SST-forced AGCM with a *cp*HM. Laguna Mar Chiquita's strong sensitivity to the recent precipitation anomaly observed in the region makes this hydrologic system particularly well adapted to such an investigation.

Comparing LMDz values against observations, our results reveal that the AGCM captures the characteristics of observed climate in the catchment. In particular, regions LA and LB follow the observed annual climate cycle fairly well. After the SD, precipitation and temperature in regions LA and LB are in better agreement with observations on annual and seasonal scales. The interannual-to-decadal variability of streamflow is well depicted by the AGCM-SD-*cp*HM model chain. We emphasize that the regions LA-SD and LB-SD discharge simulations agree reasonably well regarding the multi-decadal cycles and interannual variations in observed discharges over the Sali-Dulce Basin.

Hence, the lake model driven by regions LA-SD- and LB-SD-simulated discharges reproduces the leading modes of level variations in Laguna Mar Chiquita, such as the level rise in the 1970s and the subsequent high levels.

The levels of agreement between the observed and simulated multi-decadal variability in level variations in Laguna Mar Chiquita by the model chain underline the potential importance of multi-decadal-scale lake level climatic fluctuations, and indicate that these may be predictable by the SST forced AGCM-SD outputs. The findings coincide with previous studies conducted over the SESA catchments where using a spectral analysis, the near-decadal and near-bidecadal components of the Paranà-Plata Basin's discharges are found to be induced by SST anomalies over the tropical North Atlantic (Robertson and Mechoso 1998) or even by the North Atlantic Oscillation (NAO; Labat 2005). Our results also suggest that, superimposed upon the low-frequency variations in streamflow, specific extreme hydrological events occur and coincide with the absolute maxima in the 16Y and 8Y cycles after the 1970s. Such interannual discharge anomalies are overestimated in the simulations of regions LA and LB (i.e., for the years 1981, 1992 and 2000, as shown in Fig. 5). A close analysis of the LMDz region-SD time series during these time intervals reveals extreme annual precipitation events ($\Delta P/\bar{P}_{1981-2000} = +59\,\%$ to $+120\,\%$). A likely explanation could be that abnormally wet years leading to high peak flows are related to ENSO events. The large annual discharge anomaly in 1981 might be associated with the exceptional El Niño of 1982–1983 and the subsequent anomalies of 1992 and 2000 with the moderate El Niños of 1991–1992 and 2002–2003. The high lake levels (i.e., 1984–1986; 1992–1993; 2002–2004 in Figs. 5, 7) might be a response to the El Niño influence to enhance streamflow in the Sali-Dulce Basin. The ENSO signal is often identified as a significant driver in South American climatic anomalies (Diaz et al. 1998; Grimm et al. 2000; Pezzi and Cavalcanti 2001; Paegle and Mo 2002). In addition to its effect on South America's Pacific coast, ENSO's influence on the streamflow variability in the main tributaries of La Plata River Basin is reported to be strong by many authors (Robertson and Mechoso 1998; Dettinger et al. 2000; Robertson et al. 2001). In central Argentina, the precipitation-related ENSO signal appears less pronounced and the ENSO versus streamflow correlation harder to discern (Vargas et al. 1999; Penalba and Vargas 2004; Pasquini et al. 2006). Although high hydrological events observed in the lake basin might be interpreted as a manifestation of warm ENSO events, the time periods of annual hydrological anomalies are not correlated with the—El Niño years, and El Niño's influence in 1986/1987 and 1997/1998 on the LMDz streamflow and lake level simulations is conspicuously absent; therefore, it is difficult to conclude whether or not there is a significant linkage with ENSO.

From this investigation, we can however conclude that the leading modes of level variations in Laguna Mar Chiquita, such as the hydrological cycles as well as the moderately high level of the 1960s, the 1970s level rise, and the high levels in the 1960s, 1980s, 1990s and 2000s are fairly well captured by the AGCM-SD-*cp*HM model chain. Since the LMDz is only guided by observed sea surface conditions, our results highlight the role of global SST in modulating the multi-decadal variability in the hydroclimate over the Laguna Mar Chiquita region. Further, this study supports the need for a thorough investigation of the influence of interannual-to-decadal SST trends from different global oceans on the recent hydroclimatic variability observed in the lake region. This is interesting from a research perspective, as it should help to corroborate the influence of SST anomalies in the tropical Pacific Ocean (ENSO in particular) on high lake levels. This has potential future implications in characterizing physical mechanisms governing 20th century hydroclimatic variability in SESA; we therefore believe that this work is a first step in that direction.

In the context of the present study, Laguna Mar Chiquita can be thought of as an integrator of climate variability from interannual to decadal timescales in this region of South America. Such a sensitive recorder of hydroclimatic variations is of regional interest in that it provides a comprehensive way to better understand the links between climate variability and hydrological changes in the region. As such, the AGCM-SD-*cp*HM model chain is a promising approach for evaluating long-term lake level fluctuations in response to the projected climate changes, which will improve understanding of hydroclimatic variability in Southeastern South America.

Acknowledgments The work presented here was supported by a PhD grant from the French Ministry (Magali Troin), and benefited from funding from the French CNRS-INSU (PNEDC and LEFE-EVE programs, AMANCAY project) and from the French National Research Agency (program VMC, Project ANR-06-VULN-010, ESCARSEL project). This work was also part of the CLARIS-LBP Project (EC-FP7), ECOS-Sud-MINCYT (PA08U02, France–Argentina cooperation), and PIP 112-200801-00808 (CONICET). Mathieu Vrac was partly funded by the GIS REGYNA project as well as the ANR StaRMIP project.

References

Arnold JG, Srinivasan R, Muttiah RS, Williams JR (1998) Large area hydrologic modelling and assessment-part I: model development. J Am Water Resour Assoc 34:73–89

Barreiro M (2010) Influence of ENSO and the South Atlantic Ocean on climate predictability over southeastern South America. Clim Dyn 35:1493–1508

Barreiro M, Díaz N, Renom M (2014) Role of the global oceans and land–atmosphere interaction on summertime interdecadal variability over northern Argentina. Clim Dyn 42:1733–1753

Barros V, Clarke R, Silva Dias P (2000) Climate change in the La Plata Basin. In: CIMA CONICET (eds) UBA

Barros V, Doyle M, Gonzalez M, Camilloni I, Bejaran R, Caffera RM (2002) Climate variability over subtropical South America and the South American monsonn: a review. Meteorologica 27:33–58

Barros VR, Doyle ME, Camilloni IA (2008) Precipitation trends in southeastern South America: relationship with ENSO phases and with low-level circulation. Theor Appl Climatol 93:19–33

Berbery ER, Barros VR (2002) The hydrologic cycle of the La Plata basin in South America. J Hydrometeorol 3:630–645

Camilloni I, Barros V (2003) Extreme discharge events in the Parana River and their climate forcing. J Hydrol 278:94–106

Carreau J, Vrac M (2011) Stochastic downscaling of precipitation with neural networks conditional mixture models. Water Resour Res. doi:10.1029/2010WR010128

Chen J, Brissette F, Chaumont D, Braun M (2013) Finding appropriate bias correction methods in downscaling precipitation for hydrologic impact studies over North America. Water Resour Res 49:4187–4205

Déqué M (2007) Frequency of precipitation and temperature extremes over France in an anthropogenic scenario: model results and statistical correction according to observed values. Glob Planet Change 57:16–26

Dettinger MD, Cayan DR, McCabe GM, Marengo JA (2000) Multiscale streamflow variability associated with El Niño/Southern Oscillation. In: Diaz HF, Markgraf V (eds) El Niño and the Southern Oscillation-multiscale variability and global and regional impacts. Cambridge University Press, Cambridge, pp 113–146

Diaz AF, Studzinski CD, Mechoso CR (1998) Relationships between precipitation anomalies in Uruguay and southern Brazil and sea surface temperatures in the Pacific and Atlantic Oceans. J Clim 11:251–271

DosReis RJ, Dias NL (1998) Multi-season lake evaporation: energy-budget estimates and CRLE model assessment with limited meteorological observations. J Hydrol 208:135–147

Fowler HJ, Blenkinsop S, Tebaldi C (2007) Linking climate change modelling to impacts studies: recent advances in downscaling techniques for hydrological modeling. Int J Climatol 27:1547–1578

Garcia NO, Mechoso CR (2005) Variability in the discharge of South American rivers and in climate. Hydrol Sci J 50:459–478

Garcia NO, Vargas WM (1998) The temporal climatic variability in the Rio de la Plata basin displayed by the river discharge. Clim Change 38:359–379

Gassman PW, Reyes MR, Green CH, Arnold JG (2007) The soil and water assessment tool: historical development, applications, and future research directions. Trans ASABE 50(4):1211–1250

Genta JL, Perez Iribarren G, Mechoso C (1998) A recent increasing trend in the streamflow of rivers in southeastern South America. J Clim 11:2858–2862

Grimm AM, Barros VR, Doyle ME (2000) Climate variability in southern South America associated with El Niño and La Niña events. J Clim 13:35–58

Hillman G (2003) Analysis y simulacion hidrologica del sistema de Mar Chiquita. Unpublished PhD, Universidad el Cordoba, Argentina

Hourdin F, Musat I, Bony S, Braconnot P, Codron F, Dufresne JL, Fairhead L, Filiberti MA, Friedlingstein P, Grandpeix JY, Krinner G, Le Van P, Li ZX, Lott F (2006) The LMDZ4 general circulation model: climate performance and sensitivity to parameterized physics with emphasis on tropical convection. Clim Dyn 27:787–813

Huang HP, Seager R, Kushnir Y (2005) The 1976/77 transition in precipitation over the Americas and the influence of tropical sea surface temperature. Clim Dyn 24:721–740

IPCC (2007) The physical science basis. Contribution of working group I to the Fourth Assessment Report of the Intergovernmental Panel on Climate Change. In: Solomon S, Qin D, Manning M, Chen Z, Marquis M, Averyt KB, Tignor M, Miller HL (eds). Cambridge University Press

IPCC (2013) Summary for policymakers. In Stocker TF, Qin D, Plattner G-K, Tignor M, Allen SK, Boschung J, Nauels A, Xia Y, Bex V, Midgley PM (eds) Climate change 2013: the physical science basis. Contribution of working group I to the Fifth Assessment Report of the Intergovernmental Panel on Climate Change. Cambridge University Press, Cambridge

Junquas C, Vera CS, Li L, Le Treut H (2012) Summer precipitation variability over Southeastern South America in a global warming scenario. Clim Dyn 38:1867–1883

Junquas C, Vera CS, Li L, Le Treut H (2013) Impact of SST changes projected in a global warming scenario on summer rainfall in southeastern South America. Clim Dyn 40:1569–1589

Krishnamurthy V, Misra V (2010) Observed ENSO teleconnections with the South American monsoon system. Atmos Sci Lett 11:7–12

Labat D (2005) Recent advances in wavelet analyses: part 1. A review of concepts. J Hydrol 314:275–288

Liebmann B, Vera CS, Carvalho LMV, Camilloni IA, Hoerling M, Allured D, Barros VR, Baez J, Bidegain M (2004) An observed trend in central South American precipitation. J Clim 17:4357–4367

Maraun D, Wetterhall F, Ireson AM, Chandler RE, Kendon EJ, Widmann M, Brienen S, Rust HW, Sauter T, Themeßl M, Venema VKC, Chun KP, Goodess CM, Jones RG, Onof C, Vrac M, Thiele-Eich I (2010) Precipitation downscaling under climate change. Recent developments to bridge the gap between dynamical models and the end user. Rev Geophys 48(3):RG3003

Marti O, Braconnot P, Bellier J, Benshila R, Bony S, Brockmann P, Cadule P, Caubel A, Denvil S, Dufresne JL, Fairhead L, Filiberti MA, Foujols MA, Fichefet T, Friedlingstein P, Grandpeix JY, Hourdin F, Krinner G, Lévy C, Madec G, Musat I, de Nolbet N, Polcher J, Talandier C (2005) The new IPSL climate system model: IPSL-CM4. Technical Note, IPSL. http://www.dods.ipsl.jussieu.fr/omamce/IPSLCM4/DocIPSLCM4

Michelangeli PA, Vrac M, Loukos H (2009) Probabilistic downscaling approaches: application to wind cumulative distribution functions. Geophys Res Lett 36:L11708

Morton FI (1983) Operational estimates of lake evaporation. J Hydrol 66:77–100

Neitsch SL, Arnold JG, Kiniry JR, Williams JR, King KW (2002) Soil and water assessment tool theoretical documentation. Version 2000, Texas Water Resources Institutes, College Station

Neitsch SL, Arnold JG, Kiniry JR, Williams JR (2005) Soil and water assessment tool, theoretical documentation. Blackland Res. Cent., Tex. A&M, Temple

Nobre P, Marengo JA, Cavalcanti IFA, Obregon G, Barros V, Camilloni I, Campos N, Ferreira AG (2006) Seasonal-to-decadal predictability and prediction of South American climate. J Clim 19:5988–6004

Paegle JN, Mo KC (2002) Linkages between summer rainfall variability over South America and sea surface temperature anomalies. J Clim 15:1389–1407

Pasquini AI, Lecomte KL, Piovano EL, Depetris PJ (2006) Recent rainfall and runoff variability in central Argentina. Quat Int 158:127–139

Penalba OC, Vargas WM (2004) Interdecadal and interannual variations of annual and extreme precipitation over central-northeastern Argentina. Int J Climatol 24:1565–1580

Pezzi LP, Cavalcanti IFA (2001) The relative importance of ENSO and tropical Atlantic sea surface temperature anomalies for seasonal precipitation over South America: a numerical study. Clim Dyn 17:205–212

Piovano EL, Ariztegui D, Córdoba F, Cioccale M, Sylvestre F (2009) Hydrological variability in South America below the tropic of capricorn (Pampas and Eastern Patagonia, Argentina) during the last 13.0 Ka. In: Vimaux F et al (eds) Past climate variability in South America and surrounding regions. Developments in paleoenvironmental research, vol 14. doi:10.1007/978-90-481-2672-9-14

Planchon O, Rosier K (2005) Variabilité des régimes pluviométriques dans le nord-ouest de l'Argentine: problèmes posés et analyse durant la deuxième moitié du vingtième siècle. Ann Assoc Int Climatol 2:55–76

Robertson AW, Mechoso CR (1998) Interannual and decadal cycles in river flows of southeastern South America. J Clim 11:2570–2581

Robertson AW, Mechoso CR (2000) Interannual and interdecadal variability of the South Atlantic convergence zone. Mon Weather Rev 128:2947–2957

Robertson AW, Mechoso CR, Garcia NO (2001) Interannual prediction of the Paraná river. Geophys Res Lett 28:4235–4238

Seager R, Naik N, Baethgen W, Robertson A, Kushnir Y, Nakamura J, Jurburg S (2010) Tropical oceanic causes of interannual to multidecadal precipitation variability in Southeast South America over the past century. J Clim 23:5517–5539

Taschetto AS, Wainer I (2008) The impact of the subtropical South Atlantic SST on South American precipitation. Ann Geophys 26:3457–3476

Troin M, Vallet-Coulomb C, Sylvestre F, Piovano E (2010) Hydrological modelling of a closed lake (Laguna Mar Chiquita, Argentina) in the context of 20th century climatic changes. J Hydrol 393:233–244

Troin M, Vallet-Coulomb C, Piovano E, Sylvestre F (2012) Hydrological impacts of climate change: assessment of a basin-lake model applicability using contrasting climatic conditions in subtropical South America. J Hydrol 475:379–391

Troin M, Velázquez JA, Caya D, Brissette F (2015) Comparing statistical post-processing of regional and global climate scenarios for hydrological impacts assessment: a case study of two Canadian catchments. J Hydrol 520:268–288

Vargas WM, Penalba OC, Minetti JL (1999) Las precipitaciones mensuales en zonas de la Argentina y el ENOS. Un enfoque hacia problemas de decisión. Meteorológicas 24:3–22

Vera C, Díaz L (2014) Anthropogenic influence on summer precipitation trends over South America in CMIP5 models. Int J Climatol. doi:10.1002/joc.4153

Vera C, Silvestri G (2009) Precipitation interannual variability in South America from the WRCP-CMIP3 multi-model dataset. Clim Dyn 32:1003–1014

Vera C, Silvestri G, Liebmann B, Gonzalez P (2006a) Climate change scenarios for seasonal precipitation in South America from IPCC-AR4 models. Geophys Res Lett 33:L13707. doi:10.1029/2006GL025759

Vera C, Higgins W, Amador J, Ambrizzi T, Garreaud R, Gochis D, Gutzler D, Lettenmaier D, Marengo CR, Nogues-Paegle J, Silva Dias PL, Zhang C (2006b) Toward a unified view of the American monsoon systems. J Clim 19:4977–5000

Vrac M, Drobinski P, Merlo A, Herrmann M, Lavaysse C, Li L, Somot S (2012) Dynamical and statistical downscaling of the French Mediterranean climate: uncertainty assessment. Nat Hazards Earth Syst Sci 12:2769–2784. doi:10.5194/nhess-12-2769-2012

Zhou J, Lau KM (1998) Does a monsoon climate exist over South America? J Clim 11:1020–1040